

An acetylcholine alpha7 positive allosteric modulator rescues a schizophrenia-associated brain endophenotype in the 15q13.3 microdeletion, encompassing *CHRNA7*

Natalia Gass¹ PhD, Wolfgang Weber-Fahr¹ PhD, Alexander Sartorius^{1,2} MD Prof. (apl.), Robert Becker¹ MSc, Michael Didriksen³ PhD, Tine Bryan Stensbøl³ PhD, Jesper Frank Bastlund³ PhD, Andreas Meyer-Lindenberg² MD PhD Prof., Adam J. Schwarz^{4,5,6} PhD

¹ Research Group Translational Imaging, Department of Neuroimaging, Central Institute of Mental Health, Medical Faculty Mannheim, University of Heidelberg, Germany

² Department of Psychiatry and Psychotherapy, Central Institute of Mental Health, Medical Faculty Mannheim, University of Heidelberg, Germany

³ H. Lundbeck A/S, Valby, Denmark

⁴ Tailored Therapeutics - Neuroscience, Eli Lilly and Company, Indianapolis, Indiana, USA

⁵ Department of Psychological and Brain Sciences, Indiana University, Bloomington, Indiana, USA

⁶ Department of Radiology and Imaging Sciences, Indiana University, Indianapolis, Indiana, USA

Corresponding author: Natalia Gass, Department of Neuroimaging, Central Institute of Mental Health, Medical Faculty Mannheim, University of Heidelberg, J5, 68159 Mannheim, Germany; Tel: +49 0621 17032966; e-mail: natalia.gass@zi-mannheim.de

Running title: nAChA7R PAM normalizes 15q13.3 hyperconnectivity

This is the author's manuscript of the article published in final edited form as:

Gass, N., Weber-Fahr, W., Sartorius, A., Becker, R., Didriksen, M., Stensbøl, T. B., ... Schwarz, A. J. (2016). An acetylcholine alpha7 positive allosteric modulator rescues a schizophrenia-associated brain endophenotype in the 15q13.3 microdeletion, encompassing *CHRNA7*. *European Neuropsychopharmacology*, 26(7), 1150–1160. <https://doi.org/10.1016/j.euroneuro.2016.03.013>

Abstract

The 15q13.3 microdeletion copy number variation is strongly associated with schizophrenia and epilepsy. The *CHRNA7* gene, encoding nicotinic acetylcholine alpha 7 receptors (nAChA7Rs), is hypothesized to be one of the main genes in this deletion causing the neuropsychiatric phenotype. Here we used a recently developed 15q13.3 microdeletion mouse model to explore whether an established schizophrenia-associated connectivity phenotype is replicated in a murine model, and whether positive modulation of nAChA7 receptor might pharmacologically normalize the connectivity patterns. Resting-state fMRI data were acquired from male mice carrying a hemizygous 15q13.3 microdeletion (N=9) and from wild-type mice (N=9). To study the connectivity profile of 15q13.3 mice and test the effect of nAChA7 positive allosteric modulation, the 15q13.3 mice underwent two imaging sessions, one week apart, receiving a single intraperitoneal injection of either 15 mg/kg Lu AF58801 or saline. The control group comprised wild-type mice treated with saline. We performed seed-based functional connectivity analysis to delineate aberrant connectivity patterns associated with the deletion (15q13.3 mice (saline treatment) versus wild-type mice (saline treatment)) and their modulation by Lu AF58801 (15q13.3 mice (Lu AF58801 treatment) versus 15q13.3 mice (saline treatment)). Compared to wild-type mice, 15q13.3 mice evidenced a predominant hyperconnectivity pattern. The main effect of Lu AF58801 was a normalization of elevated functional connectivity between prefrontal and frontal, hippocampal, striatal, thalamic and auditory regions. The strongest effects were observed in brain regions expressing nAChA7Rs, namely hippocampus, cerebral cortex and thalamus. These effects may underlie the antiepileptic, pro-cognitive and auditory gating deficit-reversal effects of nAChA7R stimulation.

Key words: 15q13.3 microdeletion; mouse model; schizophrenia; resting-state fMRI.

1. Introduction

The 15q13.3 microdeletion copy number variation (CNV) is strongly associated with schizophrenia (OR=11.5-17.9), idiopathic generalized epilepsy (OR=68) and autism spectrum disorders (OR=∞) in humans (Dibbens et al., 2009, Moreno-De-Luca et al., 2013, Sebat et al., 2009). Cognitive deficits are also prevalent: 15q13.3 deletion carriers have an average non-verbal IQ of 60, show behavior abnormalities such as attention problems, hyperactivity and impairments in functional communication (Ziats et al., 2016).

While 25% of this microdeletion occurs *de novo*, in the majority of cases (75%) it is inherited (Hoppman-Chaney et al., 2013). The microdeletion comprises a region of approximately 1.5 megabase (million base pairs of DNA), encompassing 7 genes (*MTMR15*, *MTMR10*, *TRPM1*, *MIR211*, *KLF13*, *OTUD7A*, *CHRNA7*). Convergent evidence has led to the hypothesis that the *CHRNA7* gene, encoding nicotinic acetylcholine alpha 7 receptors (nAChA7Rs), is one of the genes in this deletion responsible for the neuropsychiatric phenotype. For example, carriers of smaller deletions, encompassing only *CHRNA7*, manifest similar phenotypes (Gillentine and Schaaf, 2015); *CHRNA7* promoter mutations downregulating transcription are associated with schizophrenia and auditory gating deficits (Leonard et al., 2002), although this mutation is a weaker predictor of the schizophrenia phenotype, thus suggesting that other 15q13.3 CNV genes also contribute to the phenotype. Schizophrenia patients have reduced levels of nAChA7Rs in the hippocampus, reticular nucleus of thalamus, dentate gyrus and frontal cortex (Rowe et al., 2015); and expression of *CHRNA7* is reduced in autism (Yasui et al., 2011).

Pharmacological stimulation of nAChA7Rs restores auditory gating deficits in schizophrenia models in rodents (Hajos and Rogers, 2010), and results in activation of the prefrontal cortex and shell of nucleus accumbens, similar to conventional antipsychotics (Hansen et al., 2007). nAChA7Rs rapidly (within just a few milliseconds) desensitize in response to a full agonist; therefore positive allosteric modulators (PAMs) seem to be an ideal approach as they do not bind to the orthosteric receptor agonist binding site, but rather act via the allosteric binding site to increase the channel conductance without affecting receptor desensitization (Type I), or reducing receptor desensitization (Type II) (Hajos and Rogers, 2010). A novel brain-penetrant PAM, Lu AF58801, has been recently developed and shown to attenuate phencyclidine-induced deficits in a novel object recognition task in rats, a paradigm which has some relevance to cognitive deficits in schizophrenia (Eskildsen et al., 2014). It belongs to Type I PAMs which facilitate transition from resting to open channel state upon binding of an agonist, increasing agonist response amplitude without significant effect on response decay rate. The compound was tested in a number of *in vitro* safety toxicology and pharmacology assays and has been

shown to be non-cytotoxic and not leading to formation of reactive oxygen species (Eskildsen et al., 2014). Also it has no effect on basal locomotion and exploratory activity in the novel object recognition task (internal Lundbeck data).

Increasingly, psychiatric disorders are being conceptualized in terms of dysregulation of extended brain networks, and aberrant connectivity between brain regions, as measured by electrophysiological or functional imaging methods, is emerging as an important biomarker (Dawson et al., 2015). Dysfunctional connectivity indicates a disruption of information flow and interaction between distinct brain regions and is thought to underlie specific symptoms. For example, auditory hallucinations in schizophrenia are hypothesized to result from disengagement of default-mode-network functional connectivity to the auditory cortex and the latter's association with the control executive network, which could assign an external origin to the hallucinated voices rather than relating them to the internal origin (Northoff, 2015). In addition, the hippocampal-prefrontal network has abnormal connectivity in schizophrenia (Esslinger et al., 2009), which may underlie the working memory deficits in that disorder.

Recently, a mouse model of the 15q13.3 deletion has been developed and described, in which mice have approximately 50% downregulation of nAChA7 receptors expression in the brain (Fejgin et al., 2014). Mice carrying 15q13.3 deletion display auditory processing deficits similar to schizophrenia, propensity to develop myoclonic seizures, impaired long-term spatial reference memory and reduced capacity to generate gamma oscillations in response to auditory stimulus (Fejgin et al., 2014).

In the current study we tested the brain connectivity profile of 15q13.3 mice to delineate systems-level brain changes that could represent a translational endophenotype and provide a platform for target validation and proof-of-mechanism studies in drug discovery. We hypothesized that positive modulation of nAChA7 receptor by the highly selective PAM Lu AF58801 could pharmacologically normalize the connectivity signature.

2. Experimental procedures

Imaging experiments were performed at the Central Institute of Mental Health in Mannheim, Germany. Mice were generated and shipped by Taconic Artemis (Köln, Germany). We investigated male mice carrying a deletion orthologous to 15q13.3 (at chromosome 7qC) (15q13.3 mice, N=10, 24-30 g; wild-type mice, N=10, 24-30 g). The 15q13.3 mice were litter-mates of the used wild-type mice.

In the previous study from Lundbeck two doses of Lu AF58801, 10 and 30 mg/kg (p.o.), were investigated in rats (Eskildsen et al., 2014). The dose of 30 mg/kg was shown to be the minimal effective dose providing ~10.000 ng/ml plasma exposure level. Since in the current study we used anesthetized mice, our strategy was to find a MRI-suitable vehicle and route of administration for mouse, which would give approximately the same exposure as the minimal effective dose in the published rat study. A preliminary exploratory exposure study was performed in C57 mice and demonstrated that the same 10.000 ng/ml exposure is reached when using the 15 mg/kg dose (i.p.).

The experimental design comprised three conditions. To test the effect of nAChA7 positive allosteric modulation on the 15q13.3 connectivity pattern, the 15q13.3 mice each underwent two imaging sessions, one week apart. In the first experimental session, saline vehicle was administered, in the second session - 15 mg/kg Lu AF58801 dissolved in 40% 2-hydroxypropyl-beta-cyclodextrin (HPbCD) (i.p.). As there could be a high risk of long-lasting carry-over effects for NACHA7 receptors activation mechanism after a single dose (Werkheiser et al., 2011), we did not use cross-over design with randomization, and hence all mice received saline in the first experimental session. In a control condition we used saline vehicle, since HPbCD does not cross the blood-brain barrier (Camargo et al., 2001). The third condition included the control group of the wild-type mice which underwent a single imaging session with saline vehicle injection (N=9).

The final number of 15q13.3 mice in the saline group was N=8, as two mice woke up during the experiment and had to be excluded. In the Lu AF58801 group the number of 15q13.3 mice was N=9 (from N=8 saline group one mouse died, so N=7 mice were the same as in the saline group, plus additional two 15q13.3 mice which woke up in saline condition).

As this is the first study to examine effects of PAM Lu AF58801 on rs-fMRI, it is an exploratory (hypothesis-generating) rather than confirmatory study. Thus no formal power or sample size estimation was performed, but the group sizes (N=8-9 per group) are typical of those used in rat fMRI experiments. The present results can be used to power future confirmatory or other experiments that build on this work.

The mice were housed under controlled conditions (19-23°C, 40-60% humidity) on a 12:12 h light-dark cycle (lights on at 7 a.m.) and underwent a 2-week adaptation period between their arrival and the start of the MRI experiments. The mice were 11-12 weeks old at the time of the imaging experiments.

All experiments were conducted according to the regulations covering animal experimentation

within the European Union (European Communities Council Directive 86/609/EEC) and within the German Animal Welfare Act. The experimental procedures were approved by the German animal welfare authorities (Regierungspräsidium Karlsruhe).

2.1. MRI acquisition

The experiments were performed using a 94/20 Bruker Biospec MRI scanner (9.4 Tesla; Bruker BioSpec, Ettlingen, Germany) with Avance III hardware, BGA12S gradient system with the maximum strength of 705 mT/m and running ParaVision® 6 software. Transmission and reception of the MR signal were achieved using an anatomically-shaped cryogenically-cooled 1H two-element surface coil (MRI CryoProbe™, Bruker BioSpec, Ettlingen, Germany).

Anesthesia was induced at 4% isoflurane in a mixture of 70% N₂/30% O₂. During positioning the mouse in the scanner (head first, prone), isoflurane concentration was reduced to ~1.5%. A 0.4 mg/kg bolus of medetomidine (0.2 ml) was injected subcutaneously. Then, isoflurane was slowly discontinued (starting 2 min after bolus and then reduced by 0.2% every min). When the isoflurane level was at 0.3%, a continuous infusion of medetomidine at 0.8 mg/kg/h was initiated, and then isoflurane was switched off.

The MRI acquisition protocol for each animal comprised a FieldMap, one rs-fMRI time series and a 3D structural dataset. Rs-fMRI was acquired following stabilization of physiological parameters after medetomidine anaesthesia induction (20 min after beginning of the continuous medetomidine administration) and 15 min after Lu AF58801 injection, corresponding to the maximal brain and plasma concentrations of Lu AF58801 (see Supplemental Material).

The rs-fMRI time series were acquired using a T₂*-weighted echo-planar imaging - free induction decay (EPI-FID) sequence with the following parameters: repetition time (TR)/echo time (TE) 1300/18 ms, flip angle 50°, 21 slices, 96x64 matrix, field of view (17.28x11.52) mm², slice thickness 0.4 mm, 400 acquisitions, acquisition time ~8.5 min.

Magnetic field (B₀) inhomogeneity was measured with a 3D double gradient echo FieldMap sequence (TR=20 ms, short TE=1.7 ms, long TE=5.7 ms) acquired before each EPI. The measured field values were then used in a pre-processing step to calculate and compensate the geometric distortions.

Structural data were acquired using rapid acquisition with refocused echoes (RARE) sequence with the following parameters: RARE factor 16, TR/TE 1200/50 ms, flip angle 180°, 225x192x96 matrix, acquisition time 23 min.

Breathing and cardiac rates were monitored using a respiration pad placed beneath the chest (Small Animal Instruments Inc., NY, USA) and a pulse oximeter attached to the tail, respectively. During EPI acquisition signals were recorded (10-ms resolution) using a signal breakout module (Small Animal Instruments Inc., NY, USA) and a 4-channel recorder (Velleman® N.V., Gavere, Belgium) together with the scanner trigger pulses for each measured brain volume.

2.2. Image pre-processing

EPI time series images were corrected for magnetic field (B_0) inhomogeneities using the FieldMap data and realigned (SPM8: <http://www.fil.ion.ucl.ac.uk/spm/software/spm8>). To minimize the effect of movement on the intensity of the signal, the estimated movement parameter vectors (from realignment step) were regressed out from each voxel (FSL, version 4.1. <http://www.fmrib.ox.ac.uk/fsl>). Next, respiratory and cardiac signals were filtered out from each voxel using Aztec software (van Buuren et al., 2009). A slice-timing correction was then applied to the images (SPM8). Then the functional data were spatially normalized (SPM8) to a mouse brain template with co-registered anatomical atlas (Dorr et al., 2008) using a three-step process: (1) linear coregistration (6 degree-of-freedom rigid-body transformation) to individual 3D structural datasets (without reslicing); (2) non-linear spatial normalization (estimate & write) of 3D datasets to atlas template; (3) normalization (write) of EPI datasets to atlas using transformation matrix from step (2).

Afterwards, the time course from cerebrospinal fluid (CSF) was filtered from the normalized images. First, a CSF mask was created for each dataset, and then its time course was extracted and filtered out (FSL). Finally the images were band-pass filtered (0.01-0.1 Hz) (Analysis of Functional Neuroimages (AFNI) version 2) (Cox, 1996).

2.3. Definition of functional ROIs

Due to the lack of an MRI-compatible mouse brain atlas with a fine grained parcellation of the cortex, we performed a group independent component analysis (ICA) decomposition on an independent cohort of C57BL/6 mice (N=10, 11-week old, 22-27g) measured under the same conditions (scanner and anesthetic protocol) to define a set of meaningful brain nodes for use as seeds in the connectivity analysis. ICA was performed using 40 components that were then thresholded to contain the top 0.5% voxels in each component map. For the seed-based analysis we selected 10 components covering the prefrontal/cingulate, hippocampal, amygdala and

sensory-related brain areas (Figure 1).

Specifically, we selected seeds that were plausibly located in the mouse brain parenchyma and comprised prefrontal/cingulate regions (orbitofrontal cortex, cingulate cortex and retrosplenial cortex), hippocampus (ventral hippocampus and subicular complex), sensory areas (auditory cortex and anterior and posterior visual cortex), amygdala (rostral basolateral amygdaloid nucleus and anterior central amygdaloid nucleus). For all non-midline regions (i.e. all seeds except prefrontal/cingulate regions) we created a contralateral counterpart and combined it with the original seed to create a bilateral seed region, as we did not expect nor hypothesize specific unilateral effects.

2.4. Seed region analyses

Mean time courses were extracted from each mouse, for each of the above 10 seed regions, and were used for seed-based functional connectivity analyses (SPM8). A time course was extracted from each normalized CSF- and band-pass-filtered unsmoothed fMRI dataset; then the image data were spatially smoothed by 0.4 mm (approximately 2 voxels in-plane). Correlation coefficients r were calculated for the extracted time courses voxel-wise and transformed to Fisher z -scores. Next, these individual subject z -score maps were fed into the second-level analysis, comprising two-sample t -tests using contrasts [1 -1] and [-1 1] to assess functional connectivity changes across the whole brain for a given seed.

We calculated two types of comparisons for each seed region:

- (1) 15q13.3 mice (saline treatment) versus wild-type mice (saline treatment);
- (2) 15q13.3 mice (Lu AF58801 treatment) versus 15q13.3 mice (saline treatment).

The obtained statistic images were corrected for multiple comparisons using family-wise error (FWE) correction (SPM8: Gaussian random-field theory correction, $p_{\text{FWE}} < 0.05$, whole-brain corrected, cluster-level inference).

3. Results

In both wild-type and 15q13.3 groups, the presence of expected connectivity networks was confirmed qualitatively by placing seeds in the orbitofrontal cortex, primary somatosensory cortex and retrosplenial cortex (see Supplemental Material, Figure S2). The observed networks are comparable to the recently reported data obtained in the mouse brain (Sforazzini et al.,

2014,Zerbi et al., 2015).

The results of the seed analysis are presented in Figures 2-5 and Table S2 (Supplemental Material). Compared to wild-type mice, 15q13.3 mice exhibited a predominant hyperconnectivity pattern. In these mice, administration of Lu AF58801 resulted in a reduced functional connectivity for most seeds, and these patterns of modulated connectivity overlapped in many brain regions with the patterns of aberrant connectivity in the 15q13.3 mice *per se*, reflecting a pharmacological reversal of the hyperconnectivity associated with the CNV mutation. Both hyper- and hypoconnectivity patterns were associated with the subicular seed in the 15q13.3 mice, and both effects were reversed by Lu AF58801 (Figure 3(B,C)).

Specifically, positive allosteric modulation of nAChA7Rs by Lu AF58801 reversed the increased functional connectivity between the following regions (Figures 2-5):

- the orbitofrontal cortex and somatosensory, motor and cingulate cortices (Figure 2);
- the cingulate cortex and the hippocampus, subicular complex, mediodorsal thalamus, and superior colliculus (Figure 2);
- the retrosplenial cortex and the hippocampus, subicular complex, periaqueductal gray, and superior colliculus (Figure 2);
- the ventral hippocampus and the caudate-putamen, lateral septal nucleus, cingulate cortex, somato-motor regions, visual and auditory cortices, subicular complex and dentate gyrus (Figures 3A);
- the subicular complex and the caudate-putamen, lateral septal nucleus (Figure 3B);
- the amygdala (central amygdaloid nucleus) and the caudate-putamen, cingulate cortex, mediodorsal thalamus and anterior amygdaloid area (Figures 4A);
- the auditory cortex and the hippocampus, cingulate cortex (Figure 4B).

The only regions where an effect of the opposite valence was observed, meaning Lu AF58801 reversed a reduced functional connectivity observed in 15q13.3 mice, was between the subicular complex and superior colliculus, periaqueductal gray and visual cortex, and within the subicular complex *per se* (Figure 3C).

Physiological parameters

Since 15q13.3 mice have an excitability phenotype and therefore might have different susceptibility to anesthesia compared to wild-type mice, we measured and analyzed the

individual physiological parameters related to anesthesia depth, such as respiratory and cardiac rates, which could in the end affect functional connectivity strength. We found that neither respiratory frequency ($p=0.659$), nor cardiac pulse ($p=0.971$) were different between the strains (IBM SPSS Statistics 20, two-sample T-test).

4. Discussion

Similarity to neuropsychiatric phenotypes

15q13.3 mice displayed a predominant hyperconnectivity profile. Hyperconnectivity is mostly reported for autism (Baribeau and Anagnostou, 2013) and implies a dysfunction of inhibitory networks. To be able to make an appropriate comparison to human neuropsychiatric phenotypes, we took into account only those studies which investigated resting-state connectivity (no task) and used drug-naïve patients.

Notably the midline cortical regions including orbitofrontal, cingulate and retrosplenial cortex had increased connectivity with the hippocampus. Hippocampal-prefrontal connectivity is aberrant in schizophrenia patients (Rotarska-Jagiela et al., 2010, Zhou et al., 2008) and is hypothesized to represent a vulnerability trait for psychosis, since it has been observed in both first-episode SZ patients and persons at risk for psychosis (Benetti et al., 2009). Also this network is relevant for working memory, prepulse inhibition and sleep which are compromised in preclinical models of schizophrenia (Dickerson et al., 2010, Phillips et al., 2012, Sigurdsson et al., 2010). The orbitofrontal cortex is thought to be involved in sensory processing, adaptive learning and goal-directed behavior – the processes compromised in schizophrenia.

Next, an increased coupling between the cingulate cortex and mediodorsal thalamus in 15q13.3 mice is another feature similar to schizophrenia findings (Klingner et al., 2014).

It should be taken into consideration that the majority of studies on schizophrenia employ subjects with chronic schizophrenia and a history of medication. Since antipsychotics and the duration of disease have profound effect on brain function and connectivity, it is important to distinguish data obtained on chronically ill medicated patients and first-episode drug-naïve schizophrenia patients. When comparing our data with connectivity patterns in first-episode drug-naïve schizophrenia patients, we have observed that the elevated connectivity within the cingulate/retrosplenial/auditory network observed in 15q13.3 mice in the present study was consistent with the increased fronto-parietal-temporal coupling in patients (Lui et al., 2010).

Taken together, our findings suggest that the observed pattern in the 15q13.3 CNV mouse line

may recapitulate a pattern of common valence-independent vulnerability markers for symptoms in psychiatric disorders.

Modulation of brain connectivity by Lu AF58801

We found that positive allosteric modulation of nAChA7 receptor in mice carrying a hemizygous 15q13.3 microdeletion could effectively reverse the elevated functional connectivity between numerous brain regions, mainly cortical, hippocampal and sensory-related regions, thus normalizing the hyperconnectivity pattern characteristic of this model.

The hippocampus was one of the key regions which showed increased connectivity with the prefrontal, frontal and retrosplenial cortices, as well as with sensory-related (auditory/visual) regions in 15q13.3 mice; Lu AF58801 reduced the hyperconnectivity in this hippocampal-prefrontal network. The over-engagement of this circuit in 15q13.3 mice might result from reduced nAChA7Rs levels and a consequent deficient inhibitory processing, which in the end could lead to network overload and memory and learning disturbances. Both 15q13.3 and *Chrna7* knock-out mice have learning deficits (Fejgin et al., 2014, Lendvai et al., 2013). Activation of nAChA7Rs by Lu AF58801 reduced cortico-hippocampal connectivity which could theoretically improve learning and memory processes. Indeed, nAChA7R stimulation improves cognitive performance both in rodents (Eskildsen et al., 2014) and humans (Olincy et al., 2006). NACHA7R activation results in Ca²⁺ influx and a consequent facilitation of neurotransmitter release (Hajos and Rogers, 2010). Also Ca²⁺ influx activates Ca²⁺-regulated second messenger signaling pathways, such as MAPK-ERK signal transduction, a pathway regulating LTP and synaptic plasticity (Hajos and Rogers, 2010). Altogether, these processes mediated by nAChA7Rs modify synaptic plasticity and are particularly relevant for cognitive function in the cortico-hippocampal circuit.

The periaqueductal gray exhibited increased coupling with the retrosplenial cortex and subiculum. Periaqueductal gray might represent a critical site in the midbrain through which epileptical seizures of brainstem origin might spread to the forebrain (Sanada et al., 2007). Interestingly, Lu AF58801 reduced this coupling exactly in the same region of periaqueductal gray where it was elevated. Similarly, the subicular complex plays a pivotal role in seizure propagation in epilepsy (O'Mara et al., 2001). In the similar manner, thalamocortical and motor cortex coupling were increased in 15q13.3 mice, and spike discharges in idiopathic generalized epilepsy are related to these networks (Pittau and Vulliemoz, 2015). Taken together, we can speculate that Lu AF58801 might also normalize the overactivation of neural networks involved

in epileptogenesis.

We also found that the connectivity between the ventral hippocampus and lateral septum – both involved in reward, fear and anxiety behavior (Sotres-Bayon et al., 2012, Talishinsky and Rosen, 2012) – was increased in 15q13.3 mice and normalized by Lu AF58801. This may also contribute to behavioural abnormalities in deletion carriers.

Most of the brain regions where we observed Lu AF58801 effects express nAChA7Rs, namely the cerebral cortex, hippocampus, thalamus, superior colliculus and striatum. nAChA7Rs are expressed at GABAergic interneurons and glutamatergic cells and enhance GABAergic inhibition. Presynaptic nAChA7Rs have been found on glutamatergic terminals where they facilitate glutamate release, which in turn increase a variety of neurotransmitters e.g. dopamine and norepinephrine (Hajos and Rogers, 2010). Post-synaptic nAChA7Rs have been found on inhibitory GABAergic interneurons where they facilitate neuronal functioning (Morales et al., 2008). A reduced number of nAChA7Rs might result in reduction of inhibition and a consequent increase in excitability could lead to the deficient sensory and overall inhibition and epilepsy (Stevens et al., 2015) and to cognitive and learning disturbances observed in schizophrenia (Feuerbach et al., 2009).

It is hypothesized that a deficient inhibitory processing might underlie the 15q13.3 neuropsychiatric phenotype due to reduced *CHRNA7* expression and impaired activation of GABAergic interneurons, but the contribution of other CNV genes to the phenotype cannot be excluded. The hyperconnectivity observed in our study in 15q13.3 mice might also result from this imbalance of inhibition-excitation processes. In line with this hypothesis, it has been demonstrated that the activation of nAChA7Rs has an antiepileptic effect via increasing presynaptic GABAergic neurotransmission (Feuerbach et al., 2009). Interestingly, mice with reduced *Chrna7* expression have less GABA_A receptors in the hippocampus, as well as reduced expression of hippocampal GAD65 (GABA synthetic enzyme) (Adams et al., 2012). Antipsychotics, such as clozapine and olanzapine, has been suggest to improve deficient inhibitory processing via a cholinergic mechanism by interaction with nAChA7Rs (Simosky et al., 2003, Simosky et al., 2008).

In addition, nAChA7Rs have neuroprotective anti-inflammatory role (Egea et al., 2015), and a reduced activation of anti-inflammatory pathway due to their lower expression could result in abnormal brain metabolism and consequently lead to altered functional coupling between the regions.

Further experiments may be helpful to extend the pharmacological mechanism associated with

the current findings, namely those potentiating endogenous phasic tone of acetylcholine at the nAChA7Rs. For example, it would be of interest to test whether a selective antagonist (e.g., methyllycaconitine (MLA)) would block the effects of Lu AF58801. However, MLA is a large molecule with poor brain penetration, especially in mice, and supporting data (e.g., *in vitro*) to guide the selection of MLA dose expected to block the PAM effect of Lu AF58801, should inform such an experiment. It would also be of interest to compare the effects of a direct nAChA7R orthosteric agonist on the connectivity signature of the 15q13.3 mice. This would address a different (albeit related) hypothesis, namely whether a tonic activation of the nAChA7Rs would affect the 15q13.3 phenotype. Design considerations for such experiments should include dose selection, since both directly activating doses (based on *in vitro* data) as well as ultra-low doses (hypothesized to act as “co-agonists” to endogenous acetylcholine) may be relevant.

Comparison with EEG activity

Our results on hyperconnectivity are consistent with electrophysiological data in 15q13.3 mice showing increased resting gamma (30-48 Hz) power (Fejgin et al., 2014). Gamma band features are of particular interest in schizophrenia since they are linked to perceptual feature binding and synchronization between brain regions (Cardin et al., 2009). Cortical gamma oscillations and therefore the synchronization between the regions, as reflected by functional connectivity, are mediated by fast-spiking interneurons that are positively modulated by nAChA7Rs (Cardin et al., 2009). Interestingly, gamma activity after auditory stimulus and the amplitude of auditory-evoked potentials are reduced in 15q13.3 mice, reminiscent of schizophrenia patients (Fejgin et al., 2014), and bringing to attention the fact that resting-state and task-evoked gamma activity might reflect different mechanisms. stimulation can increase gamma oscillations in the hippocampus (Wang et al., 2015) and is also effective in restoring auditory gating deficits characteristic of schizophrenia and 15q13.3 deletion model (Hajos and Rogers, 2010).

Notably, schizophrenia patients have a much higher incidence of cigarette smoking (>80%) compared to the general population (Miwa et al., 2011) – a fact interpreted as a form of self-medication to improve cognitive processes and sensory deficits. Indeed, nicotine transiently improves auditory gating deficits in schizophrenia patients (Hajos and Rogers, 2010). The majority of nicotine smoking studies in schizophrenia has focused on $\alpha 4\beta 2$ receptors, however nicotine also induces an increase in *CHRNA7* mRNA and protein levels to values similar to those in control non-schizophrenic smokers (Mexal et al., 2010). It can be speculated that a positive

modulation of nAChA7Rs might more meaningfully enhance cognition in schizophrenia without the addictive effects of nicotine.

Although the reduced expression of the other genes in the microdeletion region may also contribute to the aberrant electrophysiological profile of this model (Fejgin et al., 2014), the nAChA7Rs are better understood and have long been a drug discovery target. Many nAChA7R agonists have been in clinical development, but with limited clinical success. This may be due to rapid desensitisation of this receptor upon binding of orthosteric agonists, which may lead to agonist-induced receptor desensitisation. To date, clinical trials in schizophrenia with a nAChA7R positive allosteric modulator have not been reported. Positive allosteric modulators have an advantage of preventing receptor desensitization and may provide more potent activity with less of a ceiling effect. Lu AF58801 effectively reversed aberrant connectivity within many brain circuits affected in schizophrenia and involved in epileptogenesis. Based on these results, we hypothesize that Lu AF58801 would also restore memory and auditory gating deficits in 15q13.3 mice.

Limitations

Due to concerns around long-lasting carry-over effects for NACHA7 receptors activation mechanism after a single dose (Werkheiser et al., 2011), the experimental design did not include randomization, and hence all mice received saline in the first experimental session.

Another limitation of the study is that saline vehicle was used in a control condition instead of HPbCD. However HPbCD does not cross the blood-brain barrier (Camargo et al., 2001) and we can suppose that it would not have a profound effect on the brain connectivity in the compound solution.

Conclusions

In summary, a 15q13.3 CNV mouse model was shown to exhibit widespread patterns of hyperconnectivity, including many brain networks known to be dysregulated in schizophrenia and epileptiform activity. Hippocampal connectivity with the orbitofrontal/cingulate/retrosplenial cortex might represent a common valence-independent vulnerability marker. Acute treatment with the nAChA7R positive allosteric modulator Lu AF58801 reversed these effects. This mouse line may provide a useful model to explore nAChA7R-related deficits, and the present results suggest that nAChA7R positive allosteric

modulation may be a useful mechanism for their treatment.

Figure legends

Figure 1. A 3D overview of mouse brain representing seed regions used in the functional connectivity analysis. Abbreviations: Au – auditory cortex, AV – anterior visual cortex, CA –

anterior central amygdaloid nucleus, BLA – rostral basolateral amygdaloid nucleus, Cg – cingulate cortex, OFC – orbitofrontal cortex, PV – posterior visual cortex, RS – retrosplenial cortex, Sub – subicular complex, vHC – ventral hippocampus.

Figure 2. Upper panel: Maps of functional connectivity patterns for cortical (A) orbitofrontal, (B) cingulate and (C) retrosplenial cortex seeds. Coronal slice coverage in z-bregma is from -4.8 to 2.8 mm. Color coding: red - increase of functional connectivity in 15q13 mice compared to wild-type mice; blue - decrease of functional connectivity after Lu AF58801 compared to control saline-treated 15q13 mice; yellow - overlap area for reversal effect on connectivity by Lu AF58801. Maps are thresholded at $p_{FWE} < 0.05$. Abbreviations: Cg – cingulate cortex, DG – dentate gyrus, M1 – primary motor cortex, M2 – secondary motor cortex, MDT – mediodorsal thalamus, PAG – periaqueductal gray, S1 – primary somatosensory cortex, SC – superior colliculus, Sub – subicular complex.

Lower panel: Group mean correlation values were calculated from regions of connectivity reversal identified in the statistical parametric mapping, namely orbitofrontal cortex and overlapping area from (A), orbitofrontal cortex and yellow overlapping area from (B), retrosplenial cortex and yellow overlapping area from (C). The mean Pearson correlation coefficient values for a given overlapping area were extracted from the functional connectivity maps for each group (15q13.3 mice treated with Lu AF58801, 15q13.3 mice treated with saline, wild-type mice treated with saline). These values are presented as bar plots for the clear visualization of reversal of the connectivity by Lu AF58801 to the pattern resembling the wild-type mice. Vertical axis represents correlation coefficient (r) values. The error bars represent the standard error of the mean values.

Figure 3. Upper panel: Maps of functional connectivity patterns for ventral hippocampus and subicular seeds. Coronal slice coverage in z-bregma is from -4.8 to 2.8 mm. Panels (A) and (B) show hyperconnectivity in the CNV mice with respect to (A) ventral hippocampus and (B) subicular seeds. Color coding for (A) and (B): red - increase of functional connectivity in 15q13 mice compared to wild-type mice; blue - decrease of functional connectivity after Lu AF58801 compared to control saline-treated 15q13 mice; yellow - overlap area for reversal effect on connectivity by Lu AF58801. Panel (C) shows the hypoconnectivity associated with the subicular complexum in the 15q13 mice and its reversal with Lu AF58801. Color coding for (C): blue - decrease of functional connectivity in 15q13 mice compared to wild-type mice; red - increase of

functional connectivity after Lu AF58801 compared to control saline-treated 15q13 mice. Maps are thresholded at $p_{FWE} < 0.05$. Abbreviations: Au – auditory cortex, Cg – cingulate cortex, CPu – caudate-putamen, LS – lateral septal nucleus, M – motor cortex, PAG – periaqueductal gray, S1 – primary somatosensory cortex, SC – superior colliculus, Sub – subicular complex, V – visual cortex.

Lower panel: Group mean correlation values from regions of connectivity reversal identified in the statistical parametric mapping, namely ventral hippocampus and overlapping area from (A), subicular complex and yellow overlapping area from (B), subicular complex and yellow overlapping area from (C). The explanation of the calculation is the same as in the legend for the Figure 2. Vertical axis represents correlation coefficient (r) values. The error bars represent the standard error of the mean values.

Figure 4. Upper panel: Maps of functional connectivity patterns for (A) amygdala and (B) auditory cortex. Coronal slice coverage in z-bregma is from -4.8 to 2.8 mm. Color coding: red - increase of functional connectivity in 15q13 mice compared to wild-type mice; blue - decrease of functional connectivity after Lu AF58801 compared to control saline-treated 15q13 mice; yellow - overlap area for reversal effect on connectivity by Lu AF58801. Maps are thresholded at $p_{FWE} < 0.05$. Abbreviations: AA – anterior amygdaloid area; Cg – cingulate cortex, CPu – caudate-putamen, HC – hippocampus, MDT – mediodorsal thalamus, mRt – mesencephalic reticular formation.

Lower panel: Group mean correlation values from regions of connectivity reversal identified in the statistical parametric mapping, namely amygdala and overlapping area from (A), auditory cortex and yellow overlapping area from (B). The explanation of the calculation is the same as in the legend for the Figure 2. Vertical axis represents correlation coefficient (r) values. The error bars represent the standard error of the mean values.

Figure 5. Schematic illustration of connections which were normalized by Lu AF58801 administration in 15q13.3 mice. Abbreviations: Amyg – amygdala, Cg – cingulate cortex, HC – hippocampus, LS – lateral septal nucleus, M1/M2 – primary and secondary motor cortex, MDT – mediodorsal thalamus, OFC – orbitofrontal cortex, PAG – periaqueductal gray, RS – retrosplenial cortex, SC – superior colliculus, Sub – subicular complex, V – visual cortex.

References

- Adams, C.E., Yonchek, J.C., Schulz, K.M., Graw, S.L., Stitzel, J., Teschke, P.U., Stevens, K.E., 2012. Reduced Chrna7 expression in mice is associated with decreases in hippocampal markers of inhibitory function: implications for neuropsychiatric diseases. *Neuroscience* 207, 274-282.
- Baribeau, D.A., Anagnostou, E., 2013. A comparison of neuroimaging findings in childhood onset schizophrenia and autism spectrum disorder: a review of the literature. *Front. Psychiatry.* 4, 175.
- Benetti, S., Mechelli, A., Picchioni, M., Broome, M., Williams, S., McGuire, P., 2009. Functional integration between the posterior hippocampus and prefrontal cortex is impaired in both first episode schizophrenia and the at risk mental state. *Brain* 132, 2426-2436.
- Camargo, F., Erickson, R.P., Garver, W.S., Hossain, G.S., Carbone, P.N., Heidenreich, R.A., Blanchard, J., 2001. Cyclodextrins in the treatment of a mouse model of Niemann-Pick C disease. *Life Sci.* 70, 131-142.
- Cardin, J.A., Carlen, M., Meletis, K., Knoblich, U., Zhang, F., Deisseroth, K., Tsai, L.H., Moore, C.I., 2009. Driving fast-spiking cells induces gamma rhythm and controls sensory responses. *Nature* 459, 663-667.
- Cox, R.W., 1996. AFNI: software for analysis and visualization of functional magnetic resonance neuroimages. *Comput. Biomed. Res.* 29, 162-173.
- Dawson, N., Morris, B.J., Pratt, J.A., 2015. Functional brain connectivity phenotypes for schizophrenia drug discovery. *J. Psychopharmacol.* 29, 169-177.
- Dibbens, L.M., Mullen, S., Helbig, I., Mefford, H.C., Bayly, M.A., Bellows, S., Leu, C., Trucks, H., Obermeier, T., Wittig, M., Franke, A., Caglayan, H., Yapici, Z., EPICURE Consortium, Sander, T., Eichler, E.E., Scheffer, I.E., Mulley, J.C., Berkovic, S.F., 2009. Familial and sporadic 15q13.3 microdeletions in idiopathic generalized epilepsy: precedent for disorders with complex inheritance. *Hum. Mol. Genet.* 18, 3626-3631.
- Dickerson, D.D., Wolff, A.R., Bilkey, D.K., 2010. Abnormal long-range neural synchrony in a maternal immune activation animal model of schizophrenia. *J. Neurosci.* 30, 12424-12431.
- Dorr, A.E., Lerch, J.P., Spring, S., Kabani, N., Henkelman, R.M., 2008. High resolution three-dimensional brain atlas using an average magnetic resonance image of 40 adult C57Bl/6J mice. *Neuroimage* 42, 60-69.
- Egea, J., Buendia, I., Parada, E., Navarro, E., Leon, R., Lopez, M.G., 2015. Anti-inflammatory role of microglial alpha7 nAChRs and its role in neuroprotection. *Biochem. Pharmacol.* 97, 463-472.
- Eskildsen, J., Redrobe, J.P., Sams, A.G., Dekermendjian, K., Laursen, M., Boll, J.B., Papke, R.L., Bundgaard, C., Frederiksen, K., Bastlund, J.F., 2014. Discovery and optimization of Lu AF58801, a novel, selective and brain penetrant positive allosteric modulator of alpha-7 nicotinic acetylcholine receptors: attenuation of subchronic phencyclidine (PCP)-induced cognitive deficits in rats following oral administration. *Bioorg. Med. Chem. Lett.* 24, 288-293.
- Esslinger, C., Walter, H., Kirsch, P., Erk, S., Schnell, K., Arnold, C., Haddad, L., Mier, D., Opitz von Boberfeld, C., Raab, K., Witt, S.H., Rietschel, M., Cichon, S., Meyer-Lindenberg, A., 2009. Neural

mechanisms of a genome-wide supported psychosis variant. *Science* 324, 605.

Fejgin, K., Nielsen, J., Birkenow, M.R., Bastlund, J.F., Nielsen, V., Lauridsen, J.B., Stefansson, H., Steinberg, S., Sorensen, H.B., Mortensen, T.E., Larsen, P.H., Klewe, I.V., Rasmussen, S.V., Stefansson, K., Werge, T.M., Kallunki, P., Christensen, K.V., Didriksen, M., 2014. A mouse model that recapitulates cardinal features of the 15q13.3 microdeletion syndrome including schizophrenia- and epilepsy-related alterations. *Biol. Psychiatry* 76, 128-137.

Feuerbach, D., Lingenhoehl, K., Olpe, H.R., Vassout, A., Gentsch, C., Chaperon, F., Nozulak, J., Enz, A., Bilbe, G., McAllister, K., Hoyer, D., 2009. The selective nicotinic acetylcholine receptor alpha7 agonist JN403 is active in animal models of cognition, sensory gating, epilepsy and pain. *Neuropharmacology* 56, 254-263.

Gillentine, M.A., Schaaf, C.P., 2015. The human clinical phenotypes of altered CHRNA7 copy number. *Biochem. Pharmacol.* .

Hajos, M., Rogers, B.N., 2010. Targeting alpha7 nicotinic acetylcholine receptors in the treatment of schizophrenia. *Curr. Pharm. Des.* 16, 538-554.

Hansen, H.H., Timmermann, D.B., Peters, D., Walters, C., Damaj, M.I., Mikkelsen, J.D., 2007. Alpha-7 nicotinic acetylcholine receptor agonists selectively activate limbic regions of the rat forebrain: an effect similar to antipsychotics. *J. Neurosci. Res.* 85, 1810-1818.

Hoppman-Chaney, N., Wain, K., Seger, P.R., Superneau, D.W., Hodge, J.C., 2013. Identification of single gene deletions at 15q13.3: further evidence that CHRNA7 causes the 15q13.3 microdeletion syndrome phenotype. *Clin. Genet.* 83, 345-351.

Klingner, C.M., Langbein, K., Dietzek, M., Smesny, S., Witte, O.W., Sauer, H., Nenadic, I., 2014. Thalamocortical connectivity during resting state in schizophrenia. *Eur. Arch. Psychiatry Clin. Neurosci.* 264, 111-119.

Lendvai, B., Kassai, F., Szajli, A., Nemethy, Z., 2013. Alpha7 Nicotinic Acetylcholine Receptors and their Role in Cognition. *Brain Res. Bull.* 93, 86-96.

Leonard, S., Gault, J., Hopkins, J., Logel, J., Vianzon, R., Short, M., Drebing, C., Berger, R., Venn, D., Sirota, P., Zerbe, G., Olincy, A., Ross, R.G., Adler, L.E., Freedman, R., 2002. Association of promoter variants in the alpha7 nicotinic acetylcholine receptor subunit gene with an inhibitory deficit found in schizophrenia. *Arch. Gen. Psychiatry* 59, 1085-1096.

Lui, S., Li, T., Deng, W., Jiang, L., Wu, Q., Tang, H., Yue, Q., Huang, X., Chan, R.C., Collier, D.A., Meda, S.A., Pearlson, G., Mechelli, A., Sweeney, J.A., Gong, Q., 2010. Short-term effects of antipsychotic treatment on cerebral function in drug-naive first-episode schizophrenia revealed by "resting state" functional magnetic resonance imaging. *Arch. Gen. Psychiatry* 67, 783-792.

Mexal, S., Berger, R., Logel, J., Ross, R.G., Freedman, R., Leonard, S., 2010. Differential regulation of alpha7 nicotinic receptor gene (CHRNA7) expression in schizophrenic smokers. *J. Mol. Neurosci.* 40, 185-195.

Miwa, J.M., Freedman, R., Lester, H.A., 2011. Neural systems governed by nicotinic acetylcholine receptors: emerging hypotheses. *Neuron* 70, 20-33.

Morales, M., Hein, K., Vogel, Z., 2008. Hippocampal interneurons co-express transcripts encoding

the alpha7 nicotinic receptor subunit and the cannabinoid receptor 1. *Neuroscience* 152, 70-81.

Moreno-De-Luca, D., Sanders, S.J., Willsey, A.J., Mulle, J.G., Lowe, J.K., Geschwind, D.H., State, M.W., Martin, C.L., Ledbetter, D.H., 2013. Using large clinical data sets to infer pathogenicity for rare copy number variants in autism cohorts. *Mol. Psychiatry* 18, 1090-1095.

Northoff, G., 2015. Is schizophrenia a spatiotemporal disorder of the brain's resting state? *World Psychiatry*. 14, 34-35.

Olincy, A., Harris, J.G., Johnson, L.L., Pender, V., Kongs, S., Allensworth, D., Ellis, J., Zerbe, G.O., Leonard, S., Stevens, K.E., Stevens, J.O., Martin, L., Adler, L.E., Soti, F., Kem, W.R., Freedman, R., 2006. Proof-of-concept trial of an alpha7 nicotinic agonist in schizophrenia. *Arch. Gen. Psychiatry* 63, 630-638.

O'Mara, S.M., Commins, S., Anderson, M., Gigg, J., 2001. The subiculum: a review of form, physiology and function. *Prog. Neurobiol.* 64, 129-155.

Phillips, K.G., Bartsch, U., McCarthy, A.P., Edgar, D.M., Tricklebank, M.D., Wafford, K.A., Jones, M.W., 2012. Decoupling of sleep-dependent cortical and hippocampal interactions in a neurodevelopmental model of schizophrenia. *Neuron* 76, 526-533.

Pittau, F., Vulliemoz, S., 2015. Functional brain networks in epilepsy: recent advances in noninvasive mapping. *Curr. Opin. Neurol.* 28, 338-343.

Rotarska-Jagiela, A., van de Ven, V., Oertel-Knochel, V., Uhlhaas, P.J., Vogeley, K., Linden, D.E., 2010. Resting-state functional network correlates of psychotic symptoms in schizophrenia. *Schizophr. Res.* 117, 21-30.

Rowe, A.R., Mercer, L., Casetti, V., Sendt, K.V., Giaroli, G., Shergill, S.S., Tracy, D.K., 2015. Dementia praecox redux: a systematic review of the nicotinic receptor as a target for cognitive symptoms of schizophrenia. *J. Psychopharmacol.* 29, 197-211.

Sanada, M., Zheng, F., Huth, T., Alzheimer, C., 2007. Cholinergic modulation of periaqueductal grey neurons: does it contribute to epileptogenesis after organophosphorus nerve agent intoxication? *Toxicology* 233, 199-208.

Sebat, J., Levy, D.L., McCarthy, S.E., 2009. Rare structural variants in schizophrenia: one disorder, multiple mutations; one mutation, multiple disorders. *Trends Genet.* 25, 528-535.

Sforazzini, F., Schwarz, A.J., Galbusera, A., Bifone, A., Gozzi, A., 2014. Distributed BOLD and CBV-weighted resting-state networks in the mouse brain. *Neuroimage* 87, 403-415.

Sigurdsson, T., Stark, K.L., Karayiorgou, M., Gogos, J.A., Gordon, J.A., 2010. Impaired hippocampal-prefrontal synchrony in a genetic mouse model of schizophrenia. *Nature* 464, 763-767.

Simosky, J.K., Freedman, R., Stevens, K.E., 2008. Olanzapine improves deficient sensory inhibition in DBA/2 mice. *Brain Res.* 1233, 129-136.

Simosky, J.K., Stevens, K.E., Adler, L.E., Freedman, R., 2003. Clozapine improves deficient inhibitory auditory processing in DBA/2 mice, via a nicotinic cholinergic mechanism. *Psychopharmacology (Berl)* 165, 386-396.

- Sotres-Bayon, F., Sierra-Mercado, D., Pardilla-Delgado, E., Quirk, G.J., 2012. Gating of fear in prelimbic cortex by hippocampal and amygdala inputs. *Neuron* 76, 804-812.
- Stevens, K.E., Zheng, L., Floyd, K.L., Stitzel, J.A., 2015. Maximizing the effect of an alpha7 nicotinic receptor PAM in a mouse model of schizophrenia-like sensory inhibition deficits. *Brain Res.* 1611, 8-17.
- Talishinsky, A., Rosen, G.D., 2012. Systems genetics of the lateral septal nucleus in mouse: heritability, genetic control, and covariation with behavioral and morphological traits. *PLoS One* 7, e44236.
- van Buuren, M., Gladwin, T.E., Zandbelt, B.B., van den Heuvel, M., Ramsey, N.F., Kahn, R.S., Vink, M., 2009. Cardiorespiratory effects on default-mode network activity as measured with fMRI. *Hum. Brain Mapp.* 30, 3031-3042.
- Wang, Y., Wang, Z., Wang, J., Wang, Y., Henderson, Z., Wang, X., Zhang, X., Song, J., Lu, C., 2015. The modulation of nicotinic acetylcholine receptors on the neuronal network oscillations in rat hippocampal CA3 area. *Sci. Rep.* 5, 9493.
- Werkheiser, J.L., Sydserff, S., Hubbs, S.J., Ding, M., Eisman, M.S., Perry, D., Williams, A.J., Smith, J.S., Mrzljak, L., Maier, D.L., 2011. Ultra-low exposure to alpha-7 nicotinic acetylcholine receptor partial agonists elicits an improvement in cognition that corresponds with an increase in alpha-7 receptor expression in rodents: implications for low dose clinical efficacy. *Neuroscience* 186, 76-87.
- Yasui, D.H., Scoles, H.A., Horike, S., Meguro-Horike, M., Dunaway, K.W., Schroeder, D.I., Lasalle, J.M., 2011. 15q11.2-13.3 chromatin analysis reveals epigenetic regulation of CHRNA7 with deficiencies in Rett and autism brain. *Hum. Mol. Genet.* 20, 4311-4323.
- Zerbi, V., Grandjean, J., Rudin, M., Wenderoth, N., 2015. Mapping the mouse brain with rs-fMRI: An optimized pipeline for functional network identification. *Neuroimage* 123, 11-21.
- Zhou, Y., Shu, N., Liu, Y., Song, M., Hao, Y., Liu, H., Yu, C., Liu, Z., Jiang, T., 2008. Altered resting-state functional connectivity and anatomical connectivity of hippocampus in schizophrenia. *Schizophr. Res.* 100, 120-132.
- Ziats, M.N., Goin-Kochel, R.P., Berry, L.N., Ali, M., Ge, J., Guffey, D., Rosenfeld, J.A., Bader, P., Gambello, M.J., Wolf, V., Penney, L.S., Miller, R., Lebel, R.R., Kane, J., Bachman, K., Troxell, R., Clark, G., Minard, C.G., Stankiewicz, P., Beaudet, A., Schaaf, C.P., 2016. The complex behavioral phenotype of 15q13.3 microdeletion syndrome. *Genet. Med.* .

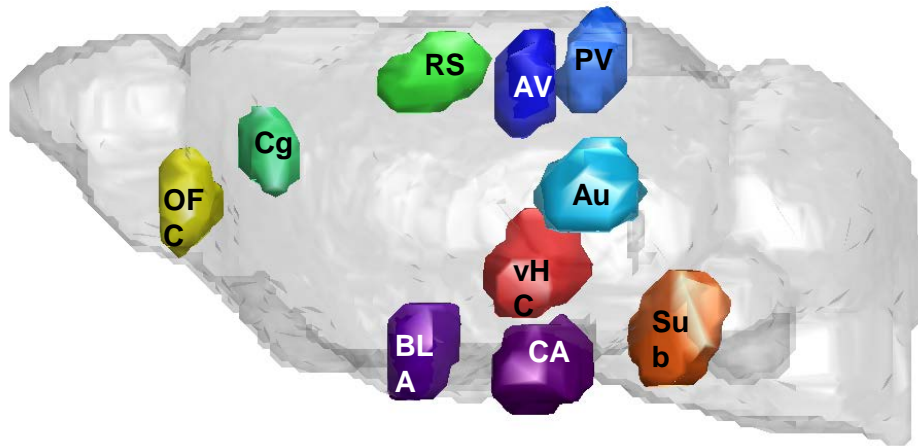
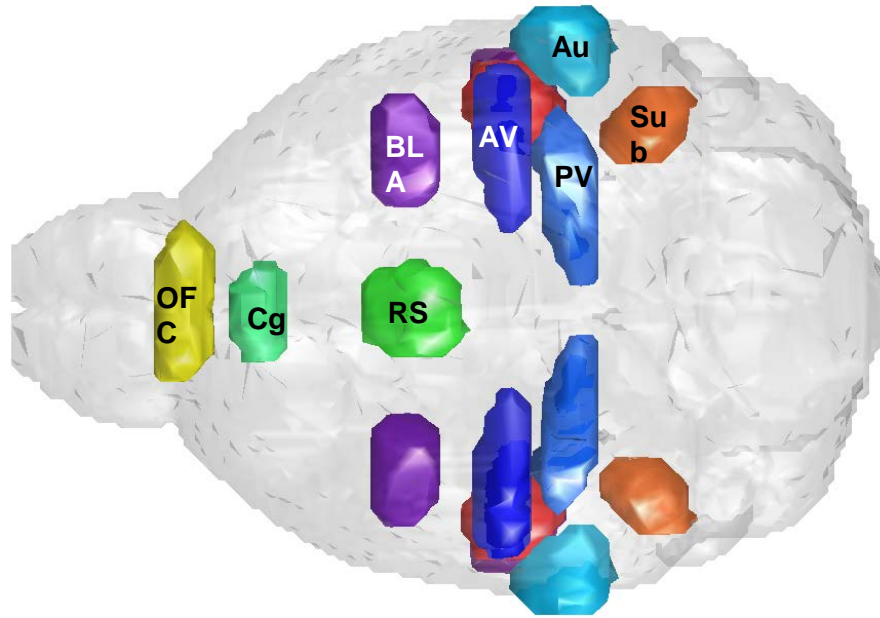
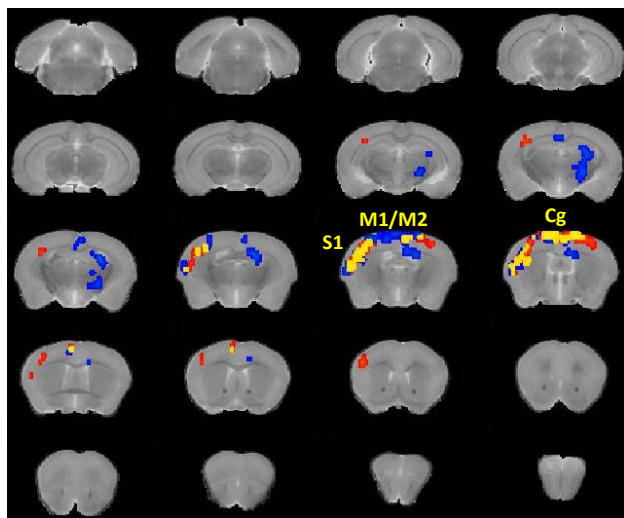
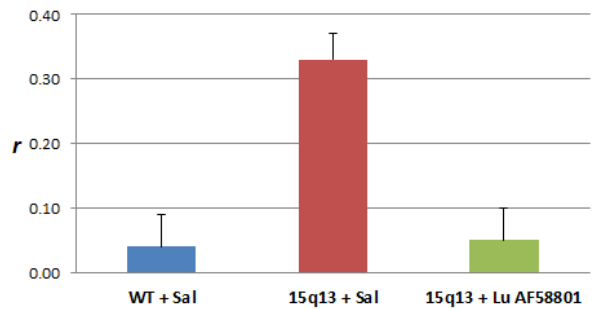


Figure 1.

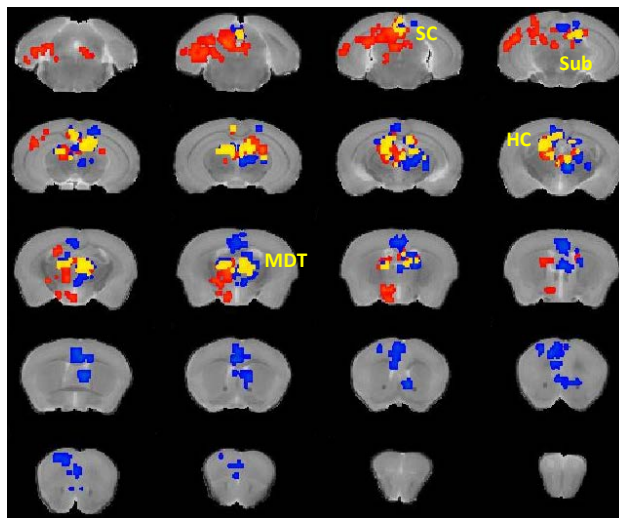
(A) Orbitofrontal cortex



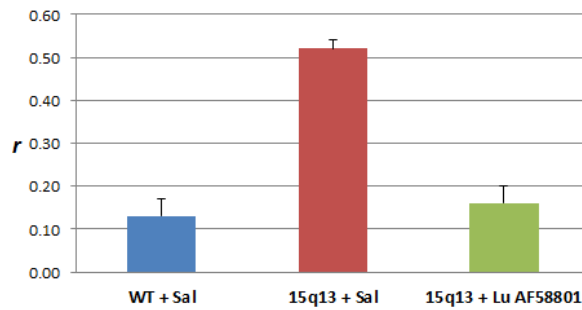
Orbitofrontal cortex



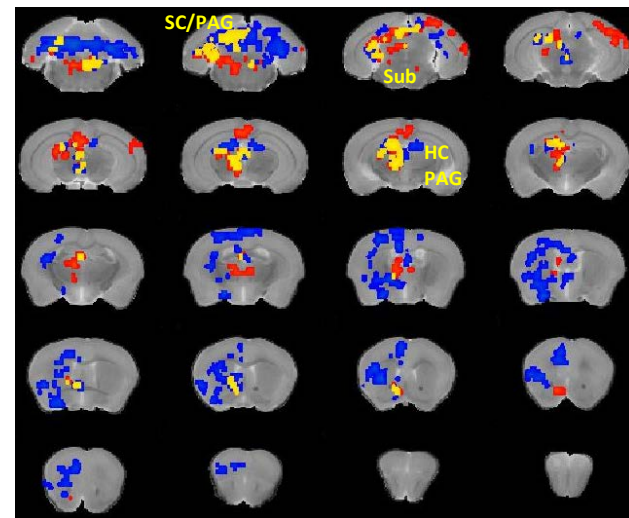
(B) Cingulate cortex



Cingulate cortex



(C) Retrosplenial cortex



Retrosplenial cortex

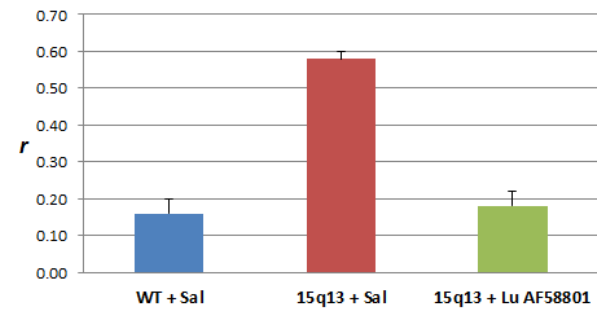
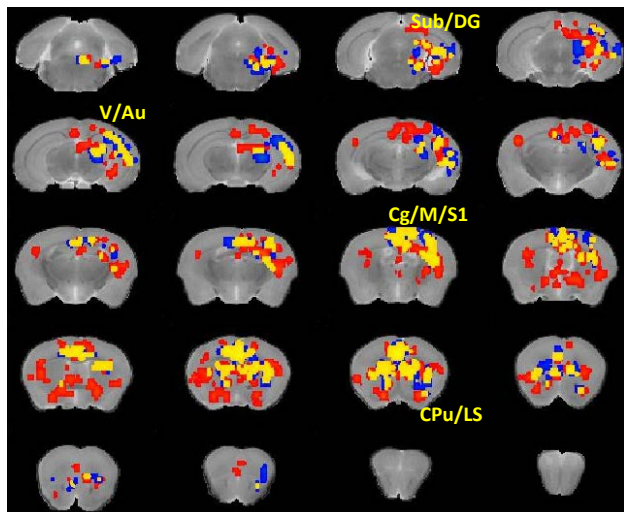
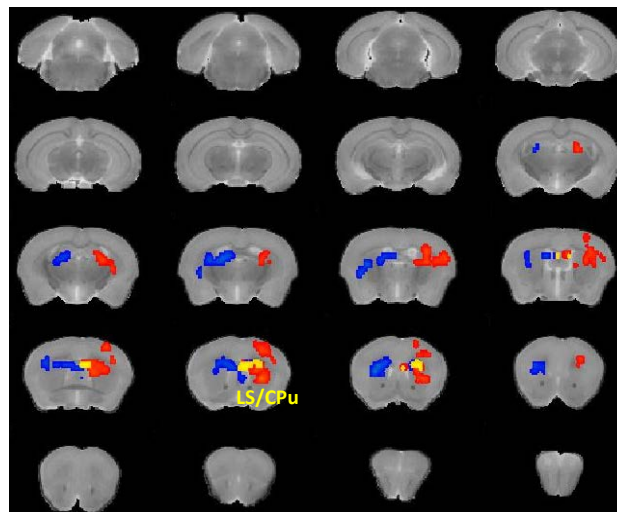


Figure 2.

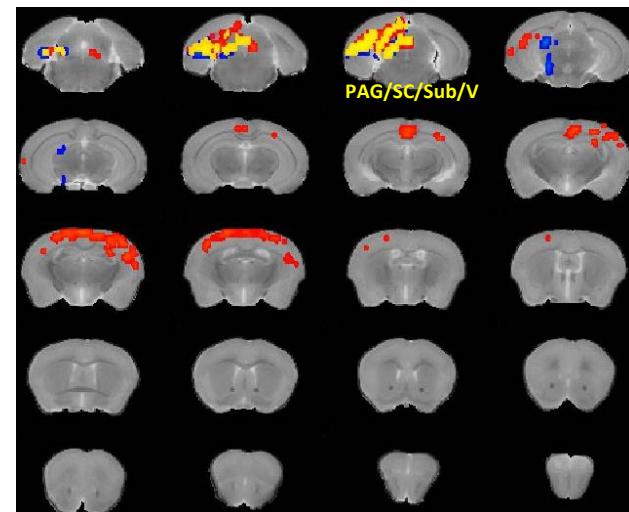
(A) Ventral hippocampus



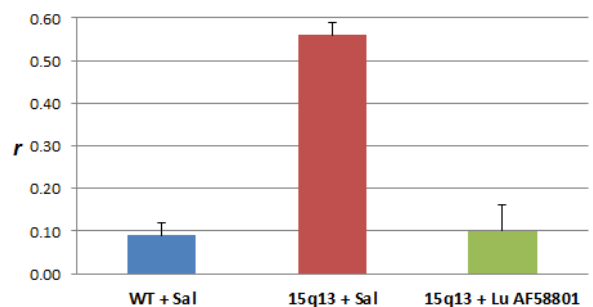
(B) Subiculum [hyperconnectivity]



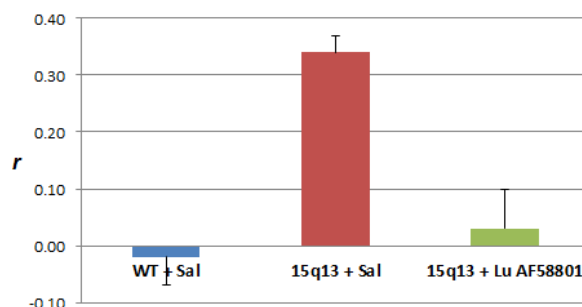
(C) Subiculum [hypoconnectivity]



Ventral hippocampus



Subiculum: hyperconnectivity



Subiculum: hypoconnectivity

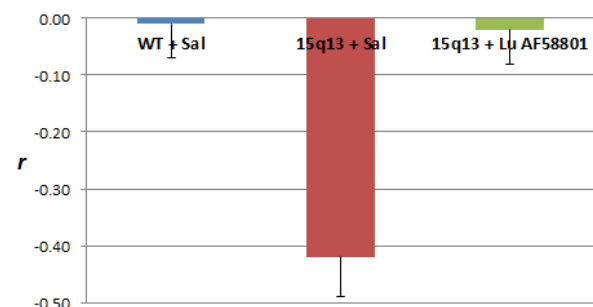


Figure 3.

(A) Amygdala

(B) Auditory cortex

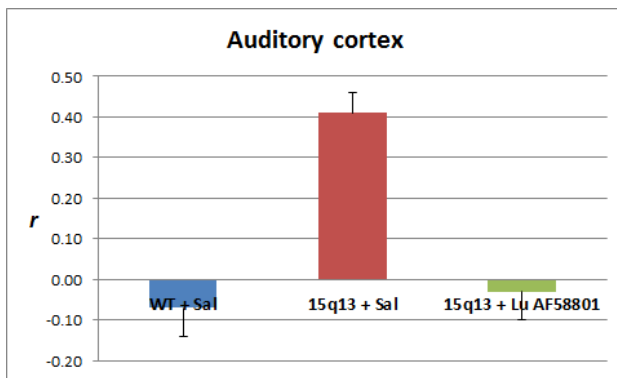
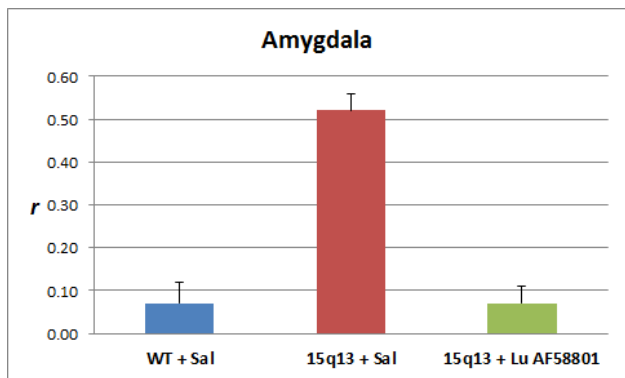
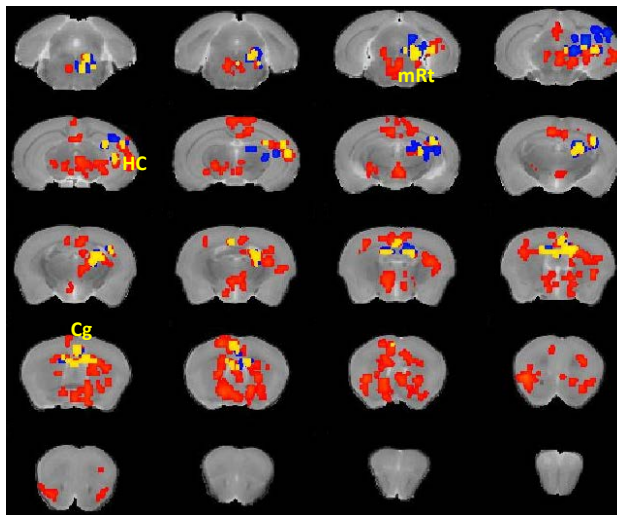
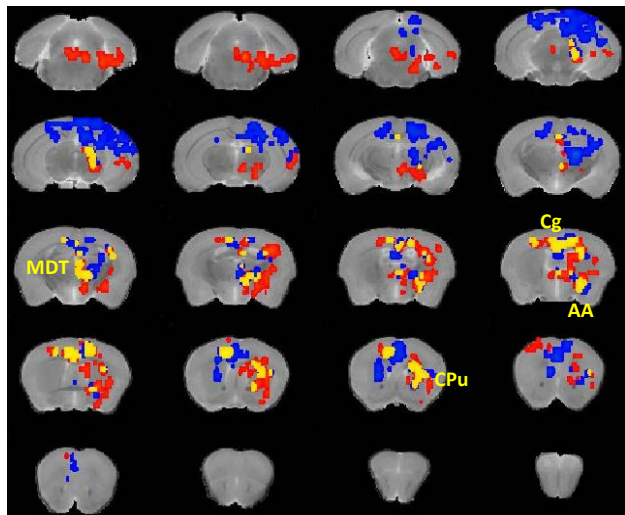


Figure 4.

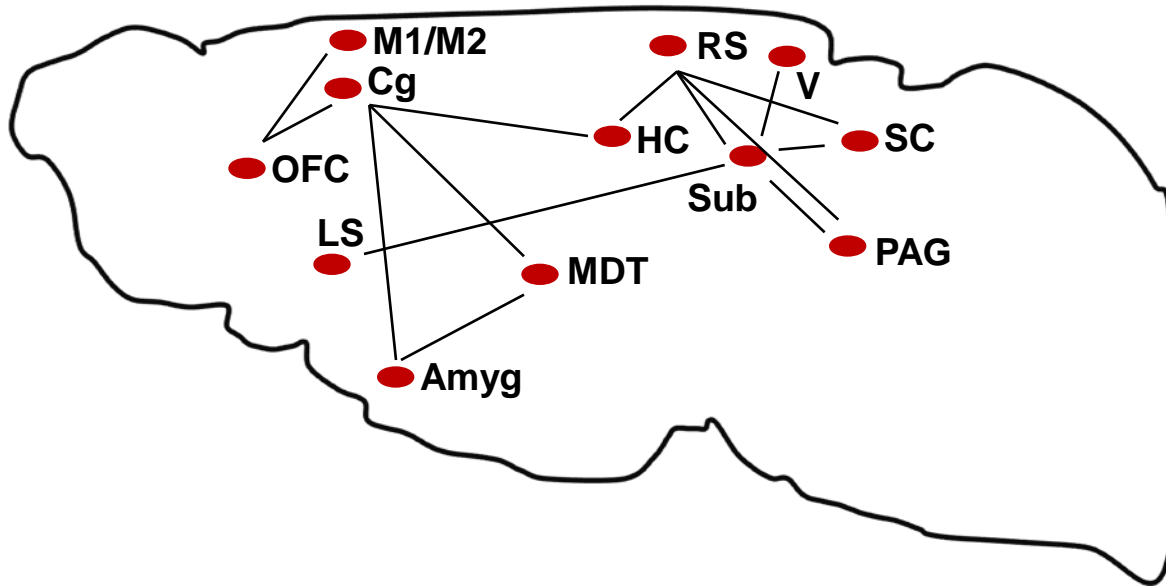


Figure 5.

Table S1. Anatomical localization (center of gravity) of seeds used in seed-based connectivity analysis. Coordinates are given in the stereotaxic space of Paxinos and Franklin (2013).

Seed region	Center of gravity coordinates		
	X (M-L) mm	Y (D-V) mm	Z (A-P) mm
Amygdala: (baso)lateral amygdaloid nucleus	0.0	-4.8	-2.5
Amygdala: central amygdaloid nucleus	0.0	-4.6	-0.9
Anterior visual cortex	-0.1	-2.8	-2.5
Auditory cortex	0.0	-2.3	-3.3
Cingulate cortex, area 24	0.0	-1.8	1.2
Orbitofrontal cortex	-0.1	-2.5	2.4
Posterior visual cortex	0.0	-0.6	-3.3
Retrosplenial cortex	-0.1	-0.7	-1.0
Subicular complex	0.0	-4.3	-4.4
Ventral hippocampus	0.0	-3.4	-2.4

Table S2. Loci of significant clusters/peak voxels obtained from seed-based connectivity analysis. Coordinates are given in the stereotaxic space of Paxinos and Franklin (2013).

Seed region	Contrast	Number of voxels in cluster	P _{FWE} cluster level	Q _{FDR} cluster level	Cluster coordinates			Anatomical localization
					X (M-L) mm	Y (D-V) mm	Z (A-P) mm	
Amygdala: (baso)lateral amygdaloid nucleus	Lu AF58801<Sal	729	0.000	0.000	0.7	-3.5	-1.8	Paracentral thalamic nucleus
Amygdala: central amygdaloid nucleus	Lu AF58801<Sal	1584	0.000	0.000	1.2	-2.6	-2.0	Lateral posterior thalamic nucleus
		545	0.006	0.003	0.7	-0.7	-0.2	Secondary motor cortex
	15q13>Wt	622	0.003	0.002	0.5	-3.5	-4.5	Isthmic reticular formation
		1132	0.000	0.000	-0.8	-1.2	0.5	Secondary motor cortex
Anterior visual cortex	15q13>Wt	923	0.000	0.000	1.2	-4.4	-1.3	Zona incerta
		510	0.009	0.004	-0.9	-0.5	-2.1	Seconadry visual cortex/retrosplenium
Auditory cortex	Lu AF58801<Sal	385	0.034	0.015	1.4	-3.2	-3.9	Mesencephalic reticular formation
		389	0.032	0.015	1.4	-2.1	-1.8	CA3 region of the hippocampus
	15q13>Wt	2096	0.000	0.000	-2.3	-3.0	1.2	Caudate-putamen
		540	0.005	0.002	0.0	-3.7	-2.7	Periaqueductal gray
Cingulate cortex, area 24	Lu AF58801<Sal	1537	0.000	0.000	0.4	-3.2	-2.0	Parafascicular thalamic nucelus
	15q13>Wt	1437	0.000	0.000	-1.1	-2.3	-3.1	Superior colliculus
Orbitofrontal cortex	Lu AF58801<Sal	588	0.005	0.004	1.6	-2.1	-1.6	CA3 region of the hippocampus
	15q13>Wt	415	0.033	0.037	-0.9	-0.5	-0.4	Primary motor cortex
Retrosplenial cortex	Lu AF58801<Sal	1125	0.000	0.000	-1.5	-4.6	-1.2	Entopeduncular nucleus
		421	0.024	0.007	-0.8	-3.2	-2.5	Periaqueductal gray
		846	0.000	0.000	-1.6	-2.6	-4.9	Sagulum nucleus
	15q13>Wt	1114	0.000	0.000	-0.8	-3.2	-2.5	Periaqueductal gray
Subicular complex	Lu AF58801<Sal	435	0.020	0.021	-1.7	-2.6	0.8	Caudate-putamen
	Lu AF58801>Sal	510	0.008	0.006	-0.6	-1.2	-4.3	Superior colliculus
		455	0.015	0.006	1.6	-0.9	-1.8	Primary somatosensory cortex

	15q13>Wt	541	0.005	0.005	0.4	-2.1	0.0	Cingulate cortex, area 24
	15q13<Wt	437	0.017	0.014	-1.7	-2.3	-3.7	Superior colliculus
Ventral hippocampus	Lu AF58801<Sal	1383	0.000	0.000	0.2	-1.2	0.5	Cingulate cortex, area 24
		799	0.000	0.000	1.6	-2.7	-2.9	Lateral posterior nucleus
	15q13>Wt	3320	0.000	0.000	1.8	-1.8	-1.0	Primary somatosensory cortex

Reference for tables S1 and S2:

Paxinos G. and Franklin K.B.J. The Mouse Brain In Stereotaxic coordinates. Academic Press, 2013.

Figure S1. Concentration of Lu AF58801 in brain (blue) and plasma (red) tested after 15 mg/kg dose (i.p.) in N=3 mice.

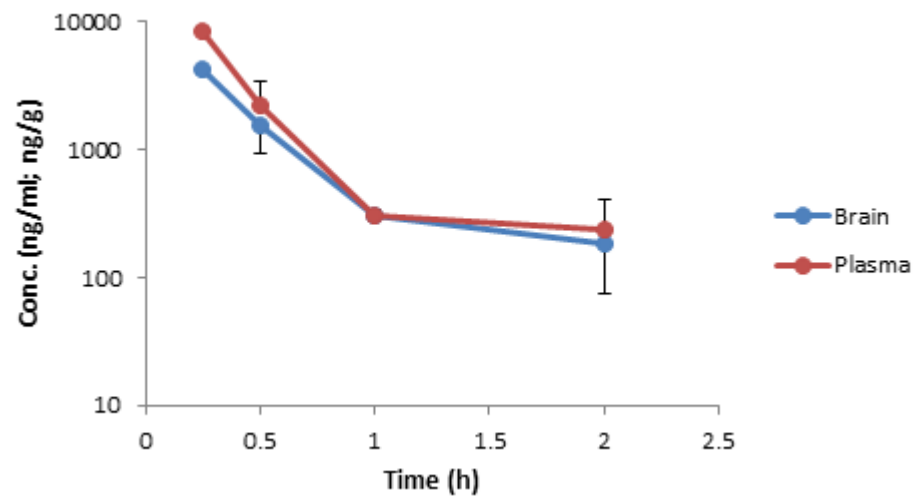
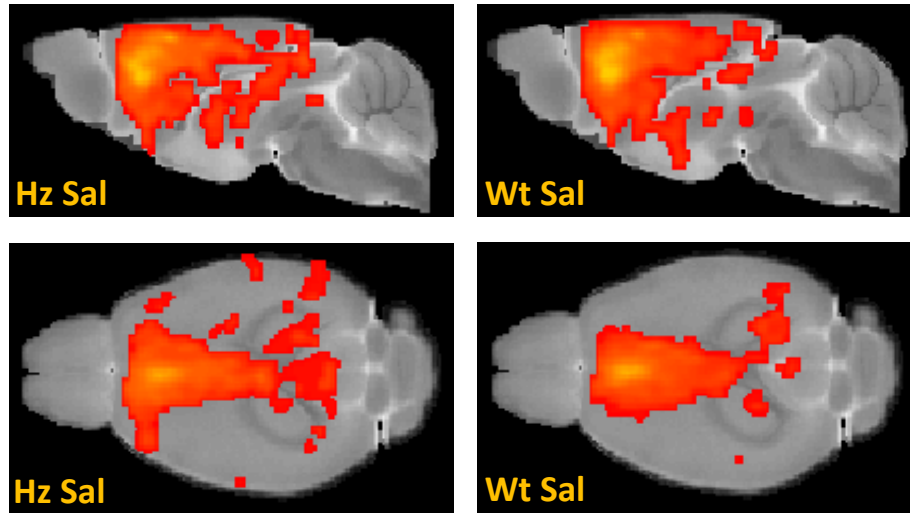
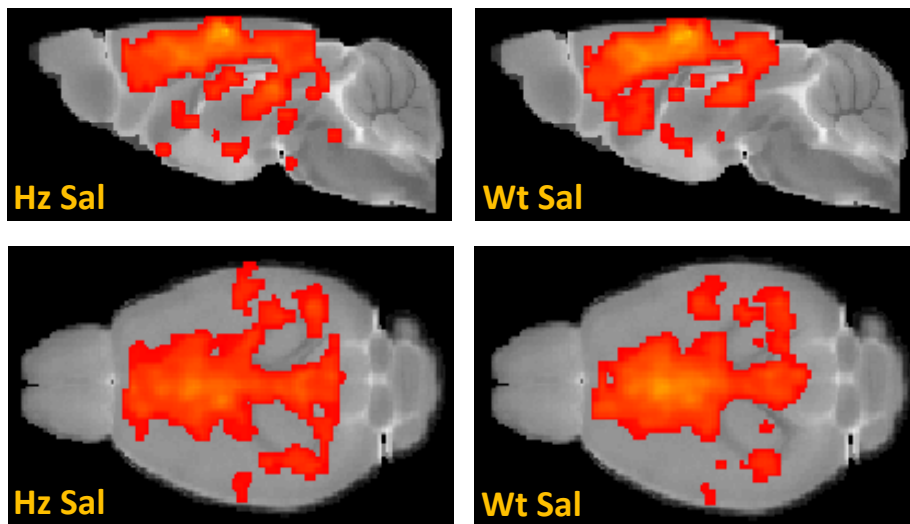


Figure S2. Functional networks for the orbitofrontal , retrosplenial and primary somatosensory cortical seeds, demonstrating the presence of expected connectivity in 15q13.3 mice comparable to wild-type mice (voxel-wise, $p < 0.001$, uncorrected). Sagittal slice is at 0.0 mm in z-bregma, transversal slice is at -1.2 mm in z-bregma.

Orbitofrontal cortex



Retrosplenial cortex



Primary somatosensory cortex

